

Genomic inference of a severe human bottleneck during the Early to Middle Pleistocene transition

Wangjie Hu^{1,2,†‡}, Ziqian Hao^{3,†}, Pengyuan Du^{1,3}, Fabio Di Vincenzo⁴, Giorgio Manzi⁵, Jialong Cui², Yun-Xin Fu^{6,7}, Yi-Hsuan Pan^{2*}, Haipeng Li^{1,8*}

Affiliations:

¹CAS Key Laboratory of Computational Biology, Shanghai Institute of Nutrition and Health, University of Chinese Academy of Sciences, Chinese Academy of Sciences; Shanghai, China.

²Key Laboratory of Brain Functional Genomics of Ministry of Education, School of Life Science, East China Normal University; Shanghai, China.

³College of Artificial Intelligence and Big Data for Medical Sciences, Shandong First Medical University & Shandong Academy of Medical Sciences; Jinan, China.

⁴Natural History Museum, University of Florence; Florence, Italy.

⁵Department of Environmental Biology, Sapienza University of Rome; Rome, Italy.

⁶Department of Biostatistics and Data Science, School of Public Health, University of Texas Health Science Center at Houston; Houston, USA.

⁷Key Laboratory for Conservation and Utilization of Bioresources, Yunnan University; Kunming, China.

⁸Center for Excellence in Animal Evolution and Genetics, Chinese Academy of Sciences; Kunming, China.

†These authors contributed equally to this work.

‡Present address: Department of Genetics and Genomic Sciences, Icahn School of Medicine at Mount Sinai; New York, USA.

*Corresponding authors. Email: yxpan@sat.ecnu.edu.cn; lihaipeng@sinh.ac.cn

This is the author's version of the work. It is posted here by permission of the AAAS for personal use, not for redistribution. The definitive version was published in *Science* on September 1, 2023, DOI: 10.1126/science.abq7487.

Click the link to download the published version: <https://doi.org/10.1126/science.abq7487>

Abstract: Population size history is essential for studying human evolution. However, ancient population size history during the Pleistocene is notoriously difficult to unravel. In this study, we developed a fast infinitesimal time coalescent process (FitCoal) to circumvent this difficulty and calculated the composite likelihood for present-day human genomic sequences of 3,154 individuals. Results showed that human ancestors went through a severe population bottleneck with about 1,280 breeding individuals between around 930 and 813 thousand years ago. The bottleneck lasted for about 117 thousand years and brought human ancestors close to extinction. The discovery of this bottleneck is congruent with a significant chronological gap in the available African and Eurasian fossil record. Our results provide new insights into our ancestry and suggest a coincident speciation event.

One-Sentence Summary: A severe bottleneck that brought human ancestors close to extinction occurred between about 930 and 813 thousand years ago.

Although the lineage of humans is estimated to have separated from that of chimpanzees and bonobos more than six million years ago, anatomically modern humans (*Homo sapiens*) are estimated to originate around 300 – 200 thousand years before the present (kyr BP) in Africa (1-3). Based on present-day human genomic sequences, the recent population size histories (i.e., the dynamics of population size since the emergence of modern humans) have been intensively studied, revealing the world-wide spread of our ancestors (4-8). However, ancient population size history of the genus *Homo* during the Pleistocene is still poorly known, although it is essential for understanding the origin of the human lineage. It is likely to be very difficult or impossible to obtain ancient DNA from African *Homo* samples dated before the emergence of *H. sapiens*. Of particular interest would be if present-day human genomic sequences could be used to infer robustly not only the recent but also the ancient population size history of humankind. Thus, a novel approach is needed to improve the inference accuracy of population size history.

Population size changes that occurred hundreds of thousands of years ago impacted the rates of coalescence and thus have left their signatures in the site frequency spectrum (SFS) of genomic sequences. The SFS is the distribution of allele frequencies in the sequences, randomly collected from the present-day human population. Each SFS category contains a certain number of mutations of the same size. As SFS is crucial for demographic inference (6, 8-12) and construction of key summary statistics (13), many efforts have been devoted to deriving its analytical formulae (14-17). However, these formulae may not achieve the required accuracy due to propagation and accumulation of numerical errors resulting from their dependence on the joint probability density function of coalescent times (16-18).

In this study, to circumvent this numerical problem, we developed the fast infinitesimal time coalescent (FitCoal) process (Fig. 1) that analytically derives expected branch length for each SFS category under arbitrary demographic models. FitCoal does not need phased haplotype data and prior information on demography. The effects of sequencing errors or hitchhiking due to positive selection can be circumvented largely by focusing on a subset of SFS that are less influenced by those factors. FitCoal was used to analyze a large number of present-day human genomic sequences from 10 African and 40 non-African populations. Results showed that our ancestors experienced a severe population bottleneck between about 930 and 813 kyr BP, most likely due to climatic changes. The average number of breeding individuals was only about 1,280 during the bottleneck period. Our findings indicate that the severe bottleneck brought the ancestral human population close to extinction and completely reshaped present-day human genetic diversity.

Results

Fast Infinitesimal Time Coalescent Process

FitCoal was developed to determine the expected branch lengths for an SFS (Fig. 1). During FitCoal analysis of a sample, the time period in which the most recent common ancestor originated was partitioned into as many time intervals as needed, such that each time interval (Δt) was very small (e.g., one month or one year). During each time interval, the population size was assumed to be constant. The probabilities of all coalescent states (i.e., all possible ancestral lineages) were calculated backward in time. For each state, the branch length during a time interval was calculated by multiplying its probability with population size and then transformed to determine the expected branch lengths. Because the expected branch length of an SFS category during a time interval was pre-calculated, FitCoal could be very fast.

FitCoal Demographic Inference

After the expected branch lengths were determined, the composite likelihood of an SFS (6, 9, 19) was calculated. FitCoal is effective for a wide range of sample sizes in the calculation of the composite likelihood of a given SFS and is much more accurate than simulation approach (fig. S1). When inferring population size history, the likelihood was maximized in a wide range of demographic scenarios. Moreover, both instantaneous and long-term exponential population changes were considered. Similar to previous studies (6, 19), the likelihood of the SFS was first maximized with the constant size model followed by repeatedly maximizing the likelihood with increased number of inference time intervals until the best model was found.

Demographic Inference from Simulated Data

The accuracy of FitCoal demographic inference was evaluated by simulation and comparison of results with those of PSMC, Stairway Plot, and SMC++ (6-8) (Fig. 2). To ensure fair comparisons, six demographic models were tested by simulating 200 independent data sets for each model as described previously (6) with the assumption that a generation time is 24 years (6, 20) and that the mutation rate is 1.2×10^{-8} per site per generation (6, 21).

Results showed that the medians of FitCoal-inferred population size histories were almost identical to the true models, and the 95% confidence intervals of FitCoal inference were narrower than those of PSMC, Stairway Plot, and SMC++ (Fig. 2). FitCoal inference accuracy could be further improved by increasing sample size and lengths of sequences (fig. S2). The proportion of the most recent changes in population size inferred from the six models showed that FitCoal could distinguish between instantaneous and exponential changes (table S1). Overall, our results confirmed that SFSs could be used to estimate population size histories (22).

It has been suggested that a population size history could be inferred using a subset of SFS or a collapsed SFS (6, 19); the latter is an SFS with high frequency mutations combined into one category. Results of simulations showed that the FitCoal could still accurately determine a population size history even when a portion (10 – 90%) of an SFS was truncated (i.e., excluded for analysis) (figs. S3 to S5), thus reducing the impact of confounding factors, such as hitchhiking effect due to positive selection (fig. S6) or sequencing errors on FitCoal analyses.

Demographic Inference of African Populations

To infer population size histories of African populations, seven African populations in the 1000 Genomes Project (1000GP) (23) and three African populations in the Human Genome Diversity Project – Centre d'Etude du Polymorphisme Humain (HGDP-CEPH) panel (24) were analyzed by the FitCoal (tables S2 to S4). Only autosomal non-coding regions were used to partially avoid the effect of purifying selection. To avoid hitchhiking effect due to positive selection (25), high-frequency mutations were excluded from the analysis. Results showed that all ten African populations went through a severe bottleneck (Fig. 3, figs. S7 and S8). The bottleneck was estimated to persist 117 thousand years, from 930 ± 23.52 (SEM) (range: 854–1,042) to 813 ± 11.02 (SEM) (range: 772–864) kyr BP. The average effective population size (i.e., the number of breeding individuals) (26) during the bottleneck period was determined to be $1,280 \pm 131$ (SEM) (range: 770–2,030), which was only 1.3% of its ancestral size ($98,130 \pm 8,720$; range: 58,600–135,000). To evaluate the impact of the bottleneck on current human genetic diversity, the expected pairwise nucleotide diversity was analyzed. Results showed that 65.85% of current human genetic diversity was lost because of the bottleneck.

Demographic Inference of Non-African Populations

The severe bottleneck was not directly detected in all 19 non-African populations in 1000GP and the 21 non-African populations in the HGDP-CEPH panel (Fig. 3, A to D, figs. S7 and S8, and tables S2, S5, and S6). The average ancestral population sizes of the populations in the two data sets were 20,260 (range: 18,850–22,220) and 20,030 (range: 19,060–21,850), respectively, similar to those determined in previous studies (7, 8, 24). The estimated population size started to decline around 368 (range: 175–756) and 367 (range: 167–628) kyr BP, respectively, consistent with previous findings that African and non-African divergence occurred much earlier than the out-of-Africa dispersal (7, 8, 23, 24). The inferred out-of-Africa dispersal and the recent population size expansion and reduction are consistent with those of previous studies (5-8, 23, 24).

Severe Bottleneck during the Early to Middle Pleistocene transition

The ancient severe bottleneck was directly detected in each of the 10 African populations, but in none of the 40 non-African populations. To investigate this discrepancy, simulations were performed with three demographic models, designated Bottleneck I, II, and III (Fig. 4, A to C, and figs. S9 and S10). Bottleneck I simulated the population size history of African agriculturalist populations with the ancient severe bottleneck, and Bottleneck II and III simulated that of non-African populations without and with the ancient severe bottleneck. Both Bottleneck I and II were inferred precisely in all simulated data sets (tables S7 to S9). However, no ancient severe bottleneck was detected in Bottleneck III simulations, which indicated that the out-of-Africa dispersal hinders the chance of discovering the ancient severe bottleneck. Furthermore, the ancient severe bottleneck was found to cause a discrepancy in the estimation of the population size between the Bottleneck III model and the inferred population size history after the bottleneck was relieved, suggesting a hidden effect of the ancient severe bottleneck on non-African populations (Fig. 4C, figs. S9C and S10C).

After the bottleneck was relieved, the average population size of non-African populations in 1000GP was 20,260, and that of those in HGDP-CEPH was 20,030. For African agriculturalist populations, the average population size in 1000GP was 27,080, and that of those in HGDP-CEPH was 27,440. This population size difference of 7,020 (Fig. 3, A and C) is likely due to the hidden effect of the ancient severe bottleneck on non-African populations. As the out-of-Africa dispersal existed in non-African populations but not in African populations, African populations had more lineages remaining to be traced back to the ancient severe bottleneck (fig. S11). In the analysis of the African YRI population, the minimum sample size was three individuals for detection of the severe bottleneck (fig. S12).

Since the signal for the existence of the severe bottleneck was too weak to be detected in non-African populations by the FitCoal, an R-extended FitCoal was performed. To eliminate noise effects resulting from problems such as sequencing or overfitting errors on the inference of population size history, the FitCoal-inferred recent population size history was used as a starting point for size estimation of an ancient population. With this modification, all 19 non-African populations in 1000GP were found to go through the severe bottleneck with approximately 1,450 individuals between 921 and 785 kyr BP (fig. S13 and table S10). This result is consistent with that obtained with African populations.

To further examine the severe bottleneck, a slow population reduction starting 1.5 million years ago was simulated (Fig. 4D), and the FitCoal-inferred population size histories were different from those observed in 1000GP and HDGP-CEPH populations, supporting the hypothesis that a sudden size reduction occurred at the beginning of bottleneck. Results of

simulations also showed that PSMC, SMC++, and Relate (7, 8, 27) under-estimated the severity of ancient bottleneck (Fig. 4, and figs. S14 to S17), similar to the observed cases (Fig. 3, E and F). Moreover, the inferred population declines shown in Fig. 4A were more severe than those inferred from the real data because the simulated data were generated under the assumption of a neutrally evolved single population and a homogeneous recombination rate, while humans evolved with sub-populations and heterogeneous recombination rate (28, 29). The FitCoal was not found to overestimate such severity (Fig. 4) and to falsely detect a bottleneck when examining the effects of continuous and pulsed introgressions among existing and ghost populations (figs. S18 to S21). Therefore, the discovery of the ancient severe bottleneck was not due to over fitting the data in FitCoal analyses.

Discussion

In this study, we developed the FitCoal, a model-flexible method for demographic inference. One key feature of FitCoal is that the expected branch lengths can be accurately determined for an SFS under an arbitrary demographic model, allowing precise calculation of the likelihood. Analyses by FitCoal are less time-consuming than those by other methods, such as PSMC, SMC++, Stairway Plot, and Relate, in most of cases (28/32 = 87.5%) (tables S11 and S12). By discarding rare and high-frequency mutations, FitCoal can avoid the effects of sequencing errors or hitchhiking due to positive selection without losing its inference accuracy. Because both instantaneous and exponential changes are allowed within each inference time interval, FitCoal can reveal the dynamic of population size precisely. Since coalescent events become rare when tracing backward in time, the length of inference time interval is usually set to increase progressively (6-8). Although this strategy can capture recent population size changes, it may miss ancient ones. Therefore, FitCoal inference time intervals are allowed to vary during demographic inference, and FitCoal can make a fast and accurate inference of recent and ancient population size histories.

The most important discovery with FitCoal is that human ancestors went through a severe bottleneck in the late Lower Pleistocene (Fig. 5). This ancient severe bottleneck was directly found in all 10 African populations, but only a weak signal of the existence of such was detected in all 40 non-African populations. This observation is consistent with the coalescent theory and the occurrence of the out-of-Africa dispersal. Results of our large-scale simulations demonstrated that FitCoal did not falsely infer the bottleneck due to positive selections (figs. S6 and S22) or population structure (fig. S18 to S21). As no overfitting cases were observed, and results obtained by examining different sets of genomic regions (Fig. 3, A and C, and fig. S23) were similar, the existence of the ancient severe bottleneck was ascertained.

Our results indicate that the ancient severe bottleneck lasted for approximately 117 thousand years (Fig. 5), and that about 98.7% of human ancestors were lost at the beginning of the bottleneck, thus threatening our ancestors with extinction. The estimated effective population size during the bottleneck period was only 1,280 breeding individuals, comparable to the effective population sizes of other endangered mammals (30, 31). This size (1,280) might have been over-estimated due to hidden population structure (32). Naturally occurring population size fluctuations might have further increased the extinction risk for our ancestors during the bottleneck. The bottleneck could also have increased the inbreeding level of our ancestors, thus contributing to the 65.85% loss in present-day human genetic diversity.

The ancient population size reduction that occurred around 930 kyr BP was likely driven by climatic changes during the Early to Middle Pleistocene transition (33, 34). During this transition period known as the "0.9 Ma event", glaciations were changed from predominantly short-term to

long-term events with more extreme thermic intensity, especially at the peak of glaciation. This event resulted in a decrease in marine surface temperature to the lowest during the entire transition period (33), with an inferred long period of drought and extensive wildlife turnover in Africa and Eurasia (35).

5 The existence of the ancient severe bottleneck could explain the extreme scarcity of the available hominin fossil record in Africa and Eurasia between 950 and 650 kyr BP (Fig. 5 and fig. S24). In Africa, only a few fossil specimens dated in this time period have been found, including the cranial fragments from Gombore in Ethiopia and the fossil samples from Tighenif in Algeria (36, 37). Although taxonomic status of these fossils is still not clear, they have features
10 resembling those of later fossils attributed to *H. heidelbergensis*. They are different from the coeval *H. antecessor* from a paleoanthropological site in Spain (Atapuerca, Gran Dolina), and some scholars considered *H. antecessor* as a possible alternative for the last common ancestor (LCA) (38). During the same chronological interval, the East Asian fossil record contains specimens identified as *H. erectus* (39). It does not appear that East Asian *H. erectus* is
15 connected to the ancient severe bottleneck, as it is unlikely to have contributed to the lineage leading to modern humans (38). In addition, coincident with this bottleneck, two ancestral chromosomes are believed to have fused to form chromosome 2 in humans around 900 to 740 kyr BP (40, 41). Therefore, the ancient severe bottleneck possibly marks a speciation event leading to the emergence of the LCA shared by Denisovans, Neanderthals, and modern humans,
20 whose divergence has been dated to about 765 – 550 kyr BP (38, 42, 43).

A rapid population recovery was detected in all 10 African populations with a 20-fold increase in size around 813 kyr BP. Control of fire could be part of the explanation for this population expansion as shown by the early archaeological evidence found in Israel dated about 790 kyr BP (44). Other factors, such as climatic changes (33, 34), might also be a driving force for this rapid population recovery.
25

The ancient severe bottleneck was not detected in previous SFS-based analyses (6, 10, 12, 14). This failure might be due to the use of predefined demographic models. In this study, we found that the likelihood must be accurately calculated in order to detect the severe bottleneck (fig. S1). The use of other methods, such as Stairway Plot, which may not have sufficient
30 resolution power for estimation of ancient population size history, is another possible reason for the failure (6).

Our study revealed an extremely small human population lasted for about 117 thousand years around 930 – 813 kyr BP. Many questions remain to be answered, such as the places where these individuals lived, how they overcame the catastrophic climate changes, and how the
35 ancient population remained so small for so long. Further studies are warranted to investigate these matters to obtain a more detailed picture of human evolution during the Early to Middle Pleistocene transition.

References and Notes

- 40 1. J. Galway-Witham, C. Stringer, How did *Homo sapiens* evolve? *Science* **360**, 1296-1298 (2018).
2. C. M. Schlebusch *et al.*, Southern African ancient genomes estimate modern human divergence to 350,000 to 260,000 years ago. *Science* **358**, 652-655 (2017).
- 45 3. A. Meneganzin, T. Pievani, G. Manzi, Pan-Africanism vs. single-origin of *Homo sapiens*: Putting the debate in the light of evolutionary biology. *Evol Anthropol* **31**, 199-212 (2022).

4. M. Stoneking, J. Krause, Learning about human population history from ancient and modern genomes. *Nat Rev Genet* **12**, 603-614 (2011).
5. S. Ramachandran *et al.*, Support from the relationship of genetic and geographic distance in human populations for a serial founder effect originating in Africa. *Proc Natl Acad Sci USA* **102**, 15942-15947 (2005).
6. X. M. Liu, Y. X. Fu, Exploring population size changes using SNP frequency spectra. *Nat Genet* **47**, 555-559 (2015).
7. H. Li, R. Durbin, Inference of human population history from individual whole-genome sequences. *Nature* **475**, 493-496 (2011).
- 10 8. J. Terhorst, J. A. Kamm, Y. S. Song, Robust and scalable inference of population history from hundreds of unphased whole genomes. *Nat Genet* **49**, 303-309 (2017).
9. H. Li, W. Stephan, Inferring the demographic history and rate of adaptive substitution in *Drosophila*. *PLoS Genet* **2**, e166 (2006).
10. L. Excoffier, I. Dupanloup, E. Huerta-Sánchez, V. C. Sousa, M. Foll, Robust
15 demographic inference from genomic and SNP data. *PloS Genet* **9**, e1003905 (2013).
11. R. C. Griffiths, S. Tavaré, Monte Carlo inference methods in population genetics. *Math Comput Modell* **23**, 141-158 (1996).
12. R. N. Gutenkunst, R. D. Hernandez, S. H. Williamson, C. D. Bustamante, Inferring the joint demographic history of multiple populations from multidimensional SNP frequency
20 data. *PLoS Genet* **5**, e1000695 (2009).
13. Y. X. Fu, Variances and covariances of linear summary statistics of segregating sites. *Theor Popul Biol* **145**, 95-108 (2022).
14. J. Jouganous, W. Long, A. P. Ragsdale, S. Gravel, Inferring the joint demographic history of multiple populations: Beyond the diffusion approximation. *Genetics* **206**, 1549-1567
25 (2017).
15. Y. X. Fu, Statistical properties of segregating sites. *Theor Popul Biol* **48**, 172-197 (1995).
16. A. Polanski, M. Kimmel, New explicit expressions for relative frequencies of single-nucleotide polymorphisms with application to statistical inference on population growth. *Genetics* **165**, 427-436 (2003).
- 30 17. D. Živković, T. Wiehe, Second-order moments of segregating sites under variable population size. *Genetics* **180**, 341-357 (2008).
18. A. Polanski, A. Bobrowski, M. Kimmel, A note on distributions of times to coalescence, under time-dependent population size. *Theor Popul Biol* **63**, 33-40 (2003).
19. A. Bhaskar, Y. X. Rachel Wang, Y. S. Song, Efficient inference of population size
35 histories and locus-specific mutation rates from large-sample genomic variation data. *Genome Res* **25**, 268-279 (2015).
20. A. Scally, R. Durbin, Revising the human mutation rate: implications for understanding human evolution. *Nat Rev Genet* **13**, 745-753 (2012).
21. A. Kong *et al.*, Rate of de novo mutations and the importance of father's age to disease
40 risk. *Nature* **488**, 471-475 (2012).
22. A. Bhaskar, Y. S. Song, Descartes' rule of signs and the identifiability of population demographic models from genomic variation data. *Ann Stat* **42**, 2469-2493 (2014).
23. The 1000 Genomes Project Consortium, A global reference for human genetic variation. *Nature* **526**, 68-74 (2015).
- 45 24. A. Bergström *et al.*, Insights into human genetic variation and population history from 929 diverse genomes. *Science* **367**, eaay5012 (2020).

25. J. C. Fay, C. I. Wu, Hitchhiking under positive Darwinian selection. *Genetics* **155**, 1405-1413 (2000).
26. H. C. Harpending *et al.*, Genetic traces of ancient demography. *Proc Natl Acad Sci USA* **95**, 1961-1967 (1998).
- 5 27. L. Speidel, M. Forest, S. Shi, S. R. Myers, A method for genome-wide genealogy estimation for thousands of samples. *Nat Genet* **51**, 1321-1329 (2019).
28. E. M. L. Scerri *et al.*, Did our species evolve in subdivided populations across Africa, and why does it matter? *Trends Ecol Evol* **33**, 582-594 (2018).
29. Z. Hao, P. Du, Y. H. Pan, H. Li, Fine human genetic map based on UK10K data set. *Hum Genet* **141**, 273-281 (2022).
- 10 30. H. Li *et al.*, Large numbers of vertebrates began rapid population decline in the late 19th century. *Proc Natl Acad Sci USA* **113**, 14079-14084 (2016).
31. Y. X. Chen *et al.*, Population and conservation status of a transboundary group of black snub-nosed monkeys (*Rhinopithecus strykeri*) between China and Myanmar. *Zool Res* **43**, 523-527 (2022).
- 15 32. J. Wakeley, Nonequilibrium migration in human history. *Genetics* **153**, 1863-1871 (1999).
33. M. J. Head, P. L. Gibbard, in *Early-Middle Pleistocene Transitions: The Land–Ocean Evidence*, M. J. Head, P. L. Gibbard, Eds. (Geological Society of London, London, 2005), pp. 1-18.
- 20 34. P. U. Clark *et al.*, The middle Pleistocene transition: characteristics, mechanisms, and implications for long-term changes in atmospheric pCO₂. *Quat Sci Rev* **25**, 3150-3184 (2006).
35. M. J. Head, B. Pillans, S. A. Farquhar, The Early-Middle Pleistocene transition: characterization and proposed guide for the defining boundary. *Episodes* **31**, 255-259 (2008).
36. A. Profico, F. Di Vincenzo, L. Gagliardi, M. Piperno, G. Manzi, Filling the gap. Human cranial remains from Gombore II (Melka Kunture, Ethiopia; ca. 850 ka) and the origin of *Homo heidelbergensis*. *J Anthropol Sci* **94**, 41-63 (2016).
- 30 37. A. Mounier, F. Marchal, S. Condemi, Is *Homo heidelbergensis* a distinct species? New insight on the Mauer mandible. *J Hum Evol* **56**, 219-246 (2009).
38. A. Bergström, C. Stringer, M. Hajdinjak, E. M. L. Scerri, P. Skoglund, Origins of modern human ancestry. *Nature* **590**, 229-237 (2021).
39. J.-J. Bahain *et al.*, Contribution of ESR et ESR/U-series methods to the dating of some Pleistocene sites of China. *L'Anthropologie* **121**, 215-233 (2017).
- 35 40. B. Poszewiecka, K. Gogolewski, P. Stankiewicz, A. Gambin, Revised time estimation of the ancestral human chromosome 2 fusion. *BMC Genomics* **23**, 616 (2022).
41. T. R. Dreszer, G. D. Wall, D. Haussler, K. S. Pollard, Biased clustered substitutions in the human genome: the footprints of male-driven biased gene conversion. *Genome Res* **17**, 1420-1430 (2007).
- 40 42. K. Prüfer *et al.*, The complete genome sequence of a Neanderthal from the Altai Mountains. *Nature* **505**, 43-49 (2014).
43. D. Reich *et al.*, Genetic history of an archaic hominin group from Denisova Cave in Siberia. *Nature* **468**, 1053-1060 (2010).
- 45 44. N. Goren-Inbar *et al.*, Evidence of hominin control of fire at Gesher Benot Ya'aqov, Israel. *Science* **304**, 725-727 (2004).

45. H. Li, Genomic inference of a severe human bottleneck during the Early to Middle Pleistocene transition. *Mendeley Data*, (2023); <https://doi.org/10.17632/xmf5r8nzm.3>.
46. W. Hu *et al.*, FitCoal v1.1. *Zenodo*, (2023); <https://doi.org/10.5281/zenodo.7857456>.
47. S. Myers, C. Fefferman, N. Patterson, Can one learn history from the allelic spectrum? *Theor Popul Biol* **73**, 342-348 (2008).
- 5 48. Y. X. Fu, Probability of a segregating pattern in a sample of DNA sequences. *Theor Popul Biol* **54**, 1-10 (1998).
49. R. R. Hudson, Two-locus sampling distributions and their application. *Genetics* **159**, 1805-1817 (2001).
- 10 50. Y. Wang *et al.*, Accelerated evolution of an *Lhx2* enhancer shapes mammalian social hierarchies. *Cell Res* **30**, 408-420 (2020).
51. H. Li, S. J. Meng, Z. M. Men, Y. X. Fu, Y. P. Zhang, Genetic diversity and population history of golden monkeys (*Rhinopithecus roxellana*). *Genetics* **164**, 269-275 (2003).
52. X. M. Liu, Y. X. Fu, Stairway Plot 2: demographic history inference with folded SNP frequency spectra. *Genome Biol* **21**, 280 (2020).
- 15 53. M. E. H. Pedersen, PhD thesis, University of Southampton, Southampton (2010).
54. Z. Rosen, A. Bhaskar, S. Roch, Y. S. Song, Geometry of the sample frequency spectrum and the perils of demographic inference. *Genetics* **210**, 665-682 (2018).
55. R. R. Hudson, Generating samples under a Wright-Fisher neutral model of genetic variation. *Bioinformatics* **18**, 337-338 (2002).
- 20 56. G. K. Chen, P. Marjoram, J. D. Wall, Fast and flexible simulation of DNA sequence data. *Genome Res* **19**, 136-142 (2009).
57. F. Baumdicker *et al.*, Efficient ancestry and mutation simulation with msprime 1.0. *Genetics* **220**, iyab229 (2022).
- 25 58. C. D. Campbell *et al.*, Estimating the human mutation rate using autozygosity in a founder population. *Nat Genet* **44**, 1277-1281 (2012).
59. D. F. Conrad *et al.*, Variation in genome-wide mutation rates within and between human families. *Nat Genet* **43**, 712-714 (2011).
60. A. Frankish *et al.*, GENCODE reference annotation for the human and mouse genomes. *Nucleic Acids Res* **47**, D766-D773 (2019).
- 30 61. O. Delaneau, J. Marchini, The 1000 Genomes Project Consortium, Integrating sequence and array data to create an improved 1000 Genomes Project haplotype reference panel. *Nat Commun* **5**, 3934 (2014).
62. B. N. Howie, P. Donnelly, J. Marchini, A flexible and accurate genotype imputation method for the next generation of genome-wide association studies. *PLoS Genet* **5**, e1000529 (2009).
- 35 63. The 1000 Genomes Project Consortium, An integrated map of genetic variation from 1,092 human genomes. *Nature* **491**, 56-65 (2012).
64. A. R. Boyko *et al.*, Assessing the evolutionary impact of amino acid mutations in the human genome. *PLoS Genet* **4**, e1000083 (2008).
- 40 65. Y. Kim, W. Stephan, Detecting a local signature of genetic hitchhiking along a recombining chromosome. *Genetics* **160**, 765-777 (2002).
66. H. Li, W. Stephan, Maximum-likelihood methods for detecting recent positive selection and localizing the selected site in the genome. *Genetics* **171**, 377-384 (2005).
- 45 67. Y. X. Fu, W. H. Li, Statistical tests of neutrality of mutations. *Genetics* **133**, 693-709 (1993).

68. P. Hsieh *et al.*, Model-based analyses of whole-genome data reveal a complex evolutionary history involving archaic introgression in Central African Pygmies. *Genome Res* **26**, 291-300 (2016).
69. C. M. Schlebusch, M. Jakobsson, Tales of human migration, admixture, and selection in Africa. *Annu Rev Genomics Hum Genet* **19**, 405-428 (2018).
70. P. Skoglund *et al.*, Reconstructing prehistoric African population structure. *Cell* **171**, 59-71 (2017).
71. F. Prugnolle, A. Manica, F. Balloux, Geography predicts neutral genetic diversity of human populations. *Curr Biol* **15**, R159-160 (2005).
72. Q. Ayub *et al.*, The Kalash genetic isolate: ancient divergence, drift, and selection. *Am J Hum Genet* **96**, 775-783 (2015).
73. M. Lopez *et al.*, The demographic history and mutational load of African hunter-gatherers and farmers. *Nat Ecol Evol* **2**, 721-730 (2018).
74. R. Nielsen *et al.*, Tracing the peopling of the world through genomics. *Nature* **541**, 302-310 (2017).
75. A. Durvasula, S. Sankararaman, Recovering signals of ghost archaic introgression in African populations. *Sci Adv* **6**, eaax5097 (2020).
76. P. Beerli, Effect of unsampled populations on the estimation of population sizes and migration rates between sampled populations. *Mol Ecol* **13**, 827-836 (2004).
77. F. Tajima, Statistical method for testing the neutral mutation hypothesis by DNA polymorphism. *Genetics* **123**, 585-595 (1989).
78. M. J. Head, P. L. Gibbard, Formal subdivision of the Quaternary System/Period: Past, present, and future. *Quat Int* **383**, 4-35 (2015).
79. L. E. Lisiecki, M. E. Raymo, A Pliocene-Pleistocene stack of 57 globally distributed benthic $\delta^{18}O$ records. *Paleoceanography* **20**, PA1003 (2005).
80. G. Manzi, D. Magri, M. R. Palombo, Early-Middle Pleistocene environmental changes and human evolution in the Italian peninsula. *Quat Sci Rev* **30**, 1420-1438 (2011).
81. F. Strani *et al.*, The effects of the "0.9 Ma event" on the Mediterranean ecosystems during the Early-Middle Pleistocene transition as revealed by dental wear patterns of fossil ungulates. *Quat Sci Rev* **210**, 80-89 (2019).
82. T. Mori, A. Profico, H. Reyes-Centeno, K. Harvati, Frontal bone virtual reconstruction and geometric morphometric analysis of the mid-Pleistocene hominin KNM-OG 45500 (Olorgesailie, Kenya). *J Anthropol Sci* **98**, 49-72 (2020).
83. R. Gallotti, M. Mussi, Two Acheuleans, two humankinds: From 1.5 to 0.85 ma at Melka Kunture (upper awash, Ethiopian highlands). *J Anthropol Sci* **95**, 137-181 (2017).
84. J. Shea, *Prehistoric stone tools of Eastern Africa: a guide*. (Cambridge University Press, Cambridge, UK, 2020).
85. G. Manzi, F. Mallegni, A. Ascenzi, A cranium for the earliest Europeans: Phylogenetic position of the hominid from Ceprano, Italy. *Proc Natl Acad Sci USA* **98**, 10011-10016 (2001).
86. M. Melchionna *et al.*, From smart apes to human brain boxes. A uniquely derived brain shape in late hominins clade. *Front Earth Sci* **8**, 273 (2020).
87. A. Mounier, M. Caparrós, The phylogenetic status of *Homo heidelbergensis* - a cladistic study of Middle Pleistocene hominins. *Bmsap* **27**, 110-134 (2015).
88. R. Grün *et al.*, Dating the skull from Broken Hill, Zambia, and its position in human evolution. *Nature* **580**, 372-375 (2020).

89. J. M. Bermúdez de Castro, M. Martín-Torres, A. Gómez-Robles, L. Prado, S. Sarmiento, Comparative analysis of the Gran Dolina-TD6 (Spain) and Tighennif (Algeria) hominin mandibles. *Bull Mém Soc Anthropol Paris* **19**, 149-167 (2007).
90. D. Yu *et al.*, eGPS 1.0: comprehensive software for multi-omic and evolutionary analyses. *Natl Sci Rev* **6**, 867-869 (2019).
91. G. P. Rightmire, The human cranium from Bodo, Ethiopia: evidence for speciation in the Middle Pleistocene? *J Hum Evol* **31**, 21-39 (1996).
92. G. P. Rightmire, *Homo* in the Middle Pleistocene: Hypodigms, variation, and species recognition. *Evol Anthropol* **17**, 8-21 (2008).
93. A. Mounier, S. Condemi, G. Manzi, The stem species of our species: a place for the archaic human cranium from Ceprano, Italy. *PLoS ONE* **6**, e18821 (2011).
94. G. Bräuer, in *Modern Origins*. (Springer, 2012), pp. 221-240.
95. G. Manzi, Humans of the Middle Pleistocene: The controversial calvarium from Ceprano (Italy) and its significance for the origin and variability of *Homo heidelbergensis*. *Quat Int* **411**, 254-261 (2016).
96. Y. X. Fu, Exact coalescent for the Wright-Fisher model. *Theor Popul Biol* **69**, 385-394 (2006).

Acknowledgments: We thank Daniel Živković for sharing his codes to calculate the expected branch lengths, Xiaoming Liu for providing simulation results, and Bio-Med Big Data Center at Shanghai institute of Nutrition and Health for providing computing facility.

Funding:

National Natural Science Foundation of China grant 32270674 (HL)

National Natural Science Foundation of China grant 91131010 (HL)

National Natural Science Foundation of China grant 91731304 (HL)

National Natural Science Foundation of China grant 31100273 (YHP)

National Natural Science Foundation of China grant 91631304 (YXF)

National Natural Science Foundation of China grant 32130011 (YXF)

National Natural Science Foundation of China grant 82171801 (ZH)

Strategic Priority Research Program of the Chinese Academy of Sciences grant XDPB17 (HL)

National Key Research and Development Project grant 2022YFF1203202 (HL)

National Institute of Health grant R01HG009524 (YXF)

Education Bureau of Jinan and Shandong First Medical University grant JNSX2021046 (ZH)

Key Laboratory of Brain Functional Genomics at East China Normal University grant 20SKBFGK2 (YHP, HL)

Shanghai Institute of Nutrition and Health grant JBGSRWBD-SINH-2021-10 (HL)

China Postdoctoral Science Foundation grant 2022M711978 (ZH)

Shandong Provincial Natural Science Foundation grant ZR2022QC062 (ZH)

Shandong Provincial Postdoctoral Innovation Talent Support Program grant
SDBX2022012 (ZH)

5 **Author contributions:**

Conceptualization: WH, ZH, FDV, GM, YXF, YHP, HL

Methodology: WH, ZH, YHP, HL

Software: WH, ZH, HL

Investigation: WH, ZH, PD, FDV, GM, JC, YXF, YHP, HL

10 Visualization: WH, ZH, PD, JC, FDV, GM

Funding acquisition: ZH, YXF, YHP, HL

Supervision: GM, YHP, HL

Writing: WH, ZH, PD, FDV, GM, YXF, YHP, HL

15 **Competing interests:** Authors declare that they have no competing interests.

Data and materials availability: Raw data are deposited at Mendeley (45), and FitCoal is archived at Zenodo (46). The download links for 1000GP and HGDP-CEPH data are available in table S2.

20 **Supplementary Materials**

Materials and Methods

Supplementary Text

Figs. S1 to S60

Tables S1 to S23

25 References (47–96)

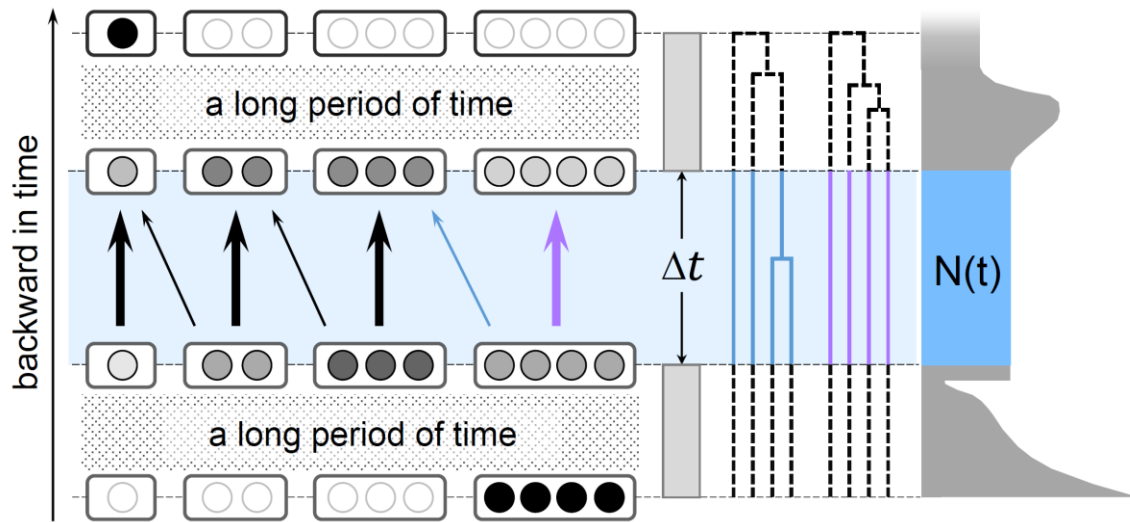


Fig. 1. Illustration of FitCoal. (Left) The backward process in which four lineages (represented by the four solid black circles at the bottom) coalesce into one (represented by the single solid black circle at the top) after passing through millions of infinitesimal time intervals (Δt). The area highlighted in blue shows the backward transformation process of different coalescent states with tiny probability changes in an infinitesimal time interval. Thick arrows indicate high transformation probabilities, and thin arrows indicate low transformation probabilities. The blue and purple arrows correlate to the two events in the middle pane represented by blue- and purple-colored lines. Each state is indicated with a box, in which one circle indicates one lineage. The boxes with solid black circles represent the states with the probability of 1. The boxes with empty circles represent the states with the probability of 0. The probabilities between 0 and 1 are represented by gray circles. (Middle) Hypothetical coalescent trees with branches of different states, indicating the number of lineages. Blue branches represent a transformation from four to three lineages. Purple branches indicate that no coalescent event occurred. (Right) The size of a theoretical population over time. The width of shadowed area denoted as $N(t)$ indicates the effective population size (i.e., the number of breeding individuals) at time t . It is assumed that the effective population size remains unchanged within a Δt .

5

10

15

20

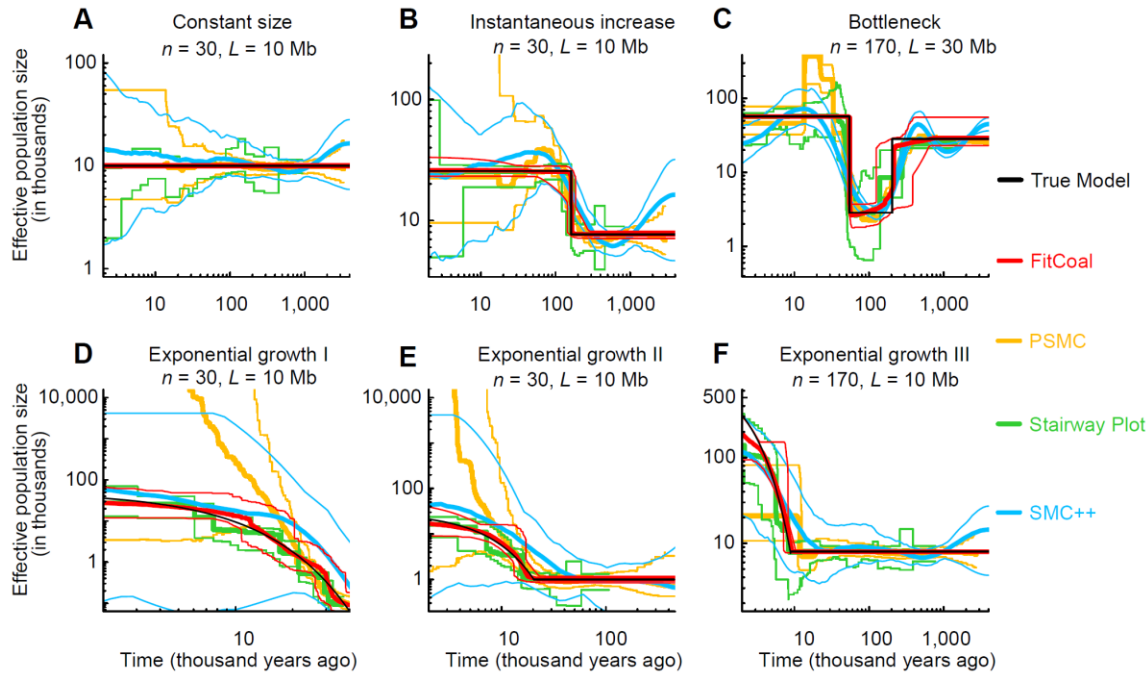


Fig. 2. Population size histories inferred by FitCoal, PSMC, Stairway Plot, and SMC++ using simulated samples. (A) Constant size model. (B) Instantaneous increase model. (C) Bottleneck model. (D) Exponential growth I model. (E) Exponential growth II model. (F) Exponential growth III model. Thin black lines indicate the true models. Thick red lines indicate the medians of FitCoal inferred population size histories; thin red lines represent 2.5 and 97.5 percentiles of FitCoal inferred population size histories. Yellow, green, and blue lines indicate results obtained with PSMC, Stairway Plot, and SMC++, respectively. The mutation rate is assumed to be 1.2×10^{-8} per base per generation, and a generation time is assumed to be 24 years. n is the number of simulated sequences, and L is the length of each simulated sequence.

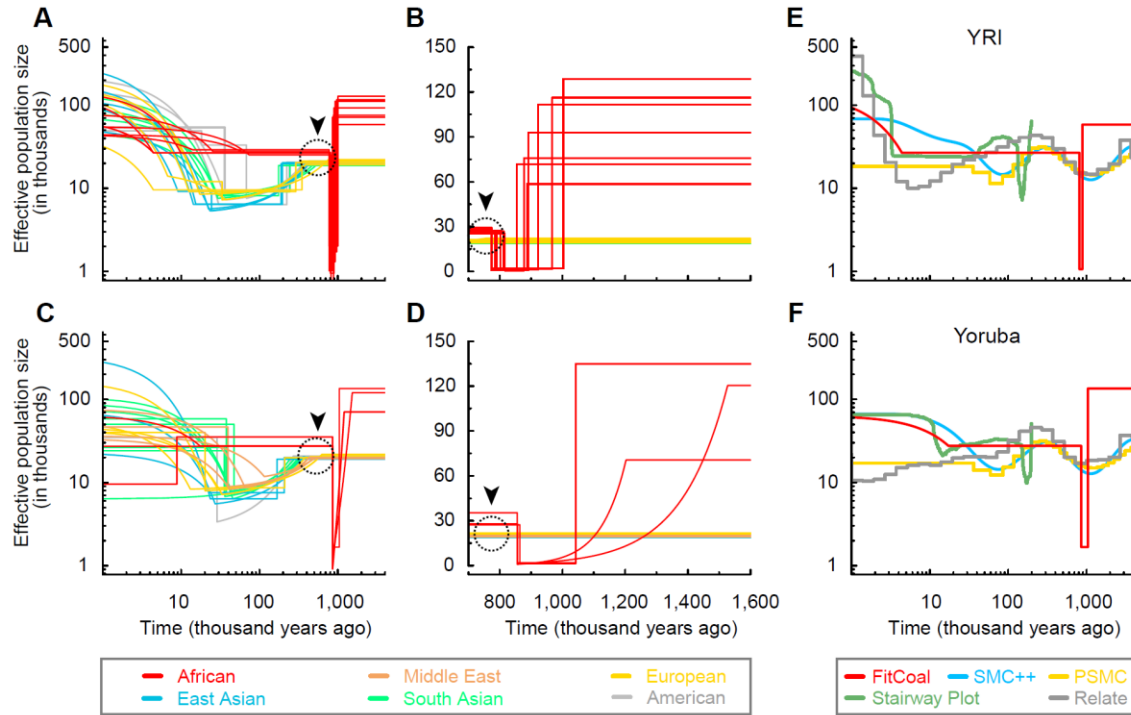


Fig. 3. FitCoal, SMC++, Stairway Plot, PSMC, and Relate inferred histories of human populations in 1000GP and HGDP-CEPH genomic datasets. The mutation rate is assumed to be 1.2×10^{-8} per base per generation, and a generation time is assumed to be 24 years. (A) Inferred population size histories of 26 populations in 1000GP. (B) Linear-scaled estimation of sizes over time of populations in 1000GP during the severe bottleneck period. (C) Inferred population size histories of 24 populations in the HGDP-CEPH panel. (D) Linear-scaled estimation of sizes over time of populations in the HGDP-CEPH panel during the severe bottleneck period. (E, F) Comparison of FitCoal, SMC++, Stairway Plot, PSMC, and Relate inferred population size histories of African YRI and Yoruba populations. Only the population size histories up to 200 kyr BP were analyzed by Stairway Plot. (A – D) Various color lines indicate the following: red, African populations; brown, Middle East populations; yellow, European populations; blue, East Asian populations; green, Central or South Asian populations; and grey, American populations. Black dashed circles with arrow heads show the discrepancy in the population size between African agriculturalist and non-African populations. (E, F) Red, blue, yellow, green, and grey lines indicate results obtained with FitCoal, SMC++, PSMC, Stairway Plot, and Relate, respectively.

20

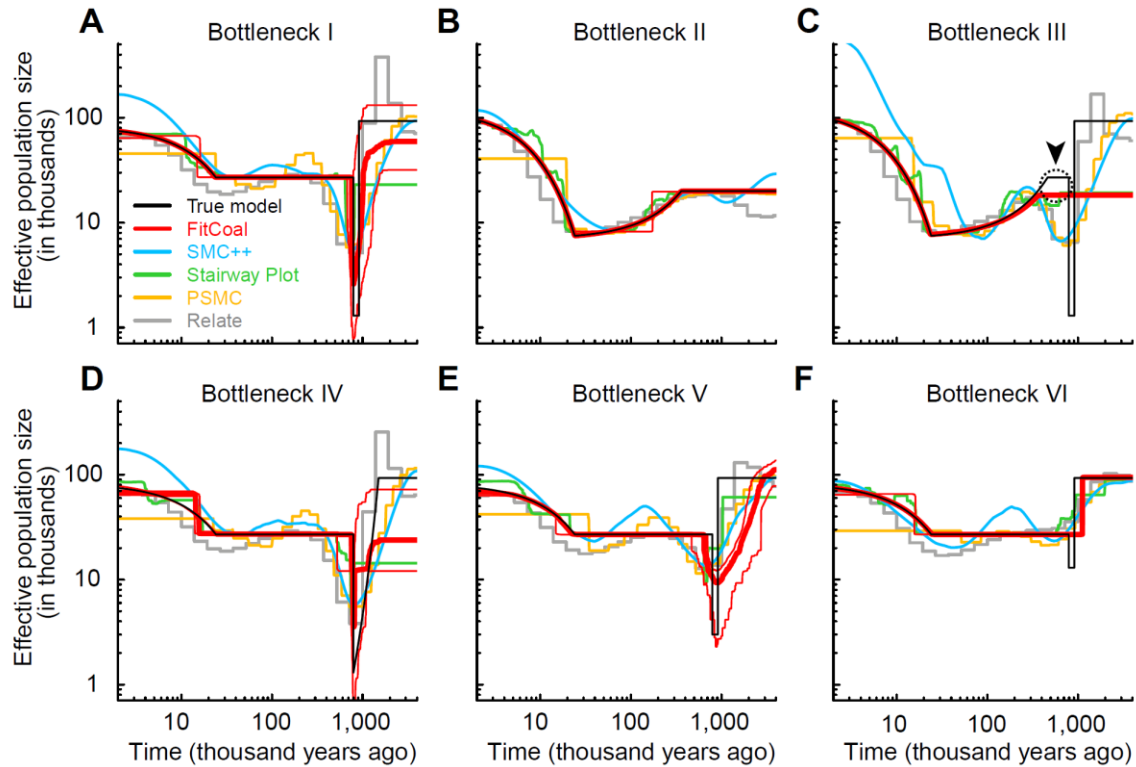


Fig. 4. Verification of the severe bottleneck. (A) Bottleneck I model, mimicking the true population size history of African agriculturalist populations. (B) Bottleneck II model, mimicking the inferred population size history of non-African populations. (C) Bottleneck III model, mimicking the true population size history of non-African populations. The gap between actual and FitCoal estimated population size is indicated by a black dashed circle and arrow head. (D) Bottleneck IV model, mimicking a population with an exponential reduction in size 1.5 million years ago. (E) Bottleneck V model, mimicking a population with a moderate bottleneck. (F) Bottleneck VI model, mimicking a population with a weak bottleneck. Black lines indicate the true models. Thick red lines denote the medians of FitCoal estimated population sizes over time; thin red lines represent 2.5 and 97.5 percentiles of FitCoal estimated population sizes over time. Blue, green, yellow, and grey lines indicate the medians of 10 runs each of SMC++, Stairway Plot, PSMC, and Relate. The mutation rate is assumed to be 1.2×10^{-8} per base per generation, and a generation time is assumed to be 24 years. Numbers of simulated sequences are 188 in Bottleneck I, IV, V, and VI and 194 in Bottleneck II and III. The length of simulated sequences is 800 Mb each.

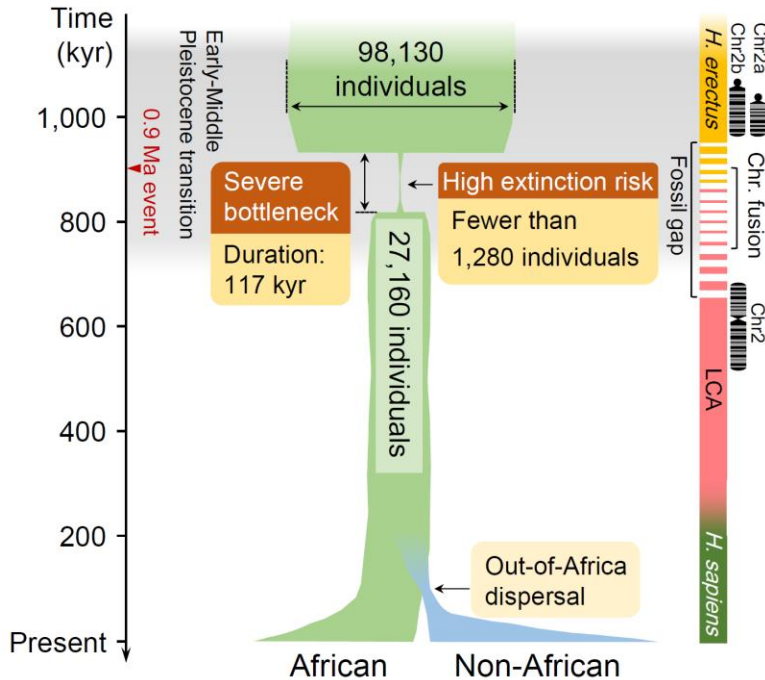


Fig. 5. Schematic diagram of human population size history. Both African (light green) and non-African (light blue) populations are presented. The width of boxes represents the effective population size (i.e., the number of breeding individuals) with naturally occurred fluctuations. The occurrence time of the out-of-Africa dispersal and the divergence between African and non-African populations are indicated. The shadowed time duration indicates the Early to Middle Pleistocene transition between 1,250 and 700 kyr BP. The red arrow indicates the peak of glaciation during the transition (i.e., the 0.9 Ma event). The ancient severe bottleneck inferred in this study is highlighted. The gap in the available African hominin fossil record and an indicative chronology for *H. erectus*, the LCA, and *H. sapiens* are shown. The estimated time period in which two ancestral chromosomes fused to become one is also shown on the right.